Direct-Current and Alternate-Decay-Current Hybrid Integrative Power Supplies Design Applied to DC Bias Treatment

Zhiwei Chen, *Member, IEEE*, Baodong Bai, *Member, IEEE*, Dezhi Chen, *Member, IEEE*, and Wenping Chai

***Abstract*—This paper proposes a novel kind of direct-current and alternate-decay-current hybrid integrative magnetization and demagnetization power supplies applied to transformer dc bias treatment based on a nanocomposite magnetic material. First, according to the single-phase transformer structure, one dc bias magnetic compensation mechanism was provided. The dc bias flux in the transformer main core could be eliminated directionally by utilizing the material remanence. Second, for the rapid response characteristic of the magnetic material to an external magnetic field, one positive and negative dc magnetization superimposed decaying ac demagnetization hybrid integrative power supplies based on single-phase rectifier circuit and inverter circuit was designed. In order to accurately control the magnetic field strength by which a good de/-magnetization effect could be achieved, this paper adopts the double-loop control technology of the magnetic field strength and magnetizing current for the nanocomposite magnetic state adjustment. Finally, two 10 kVA transformers and the experiment module of the hybrid integrative power supplies were manufactured and built. Experimental results showed that the integrated power supplies have good de/-magnetization effect and practicability, proving the validity and feasibility of the proposed scheme.**

***Index Terms*—Demagnetization, inverter circuit, magnetic material, power supply, rectifier circuit.**

I. Introduction

In RECENT years, magnetic material has played an increasingly important role in the social development. It is the main auxiliary product of all kinds of electronic products, which is indispensable not only for the home appliances including computer and communication equipment, but for the industrial products such as automobile and defense industry [1], [2]. There are many kinds of magnetic materials. Among them, the soft magnetic materials and hard magnetic materials are the most widely used in each area [3]–[5]. The magnetization and demagnetization (MD) devices are indispensable devices in the process of producing and developing magnetic material products. The MD ability is an important factor, which is used to develop the performance of all magnetic materials. With the development of the embedded technology, power electronic technology, and computer technology, MD devices start to develop with a trend of high performance, multifunction, automation, and intelligence.

In practical applications, different MD power supplies have different applications [6], [7]. Among the many MD devices, the ac/dc power supply based on the power electronic technology is widely used [8], [9]. Stable dc output can be utilized to magnetize the magnet. When the dc flows through the coil, the magnetized coil generates a constant magnetic field, which is used to complete magnet magnetization [10]. For the demagnetization, the demagnetizing field can be obtained by many methods such as the thermal demagnetization, ac demagnetization, and dc demagnetization [11]. As for the thermal demagnetization, it is not conducive to maintain the original material performance exactly and also has defects of the control difficulties. Because the magnetic material has been assembled into the product components, the difficulty of demagnetization is greater and the influence of all the parts should be taken into consideration. Applications of the thermal demagnetization method are relatively limited [12]. DC demagnetization is realized with the help of the reversing switch. The magnetization curve has a larger difference. This demagnetization method is not easy to retain the consistency of the demagnetization process, which can only eliminate most of the magnetism [13], [14]. The dc demagnetization method is suitable for circumstances where the demagnetization requirement is not very high. Fig. 1(a) shows the dc demagnetization method. If one magnet is required to achieve an ideal demagnetization state, this kind of occasion should adopt the ac demagnetization method. A magnetic field with variable intensity and direction is usually adopted and added to the magnet for demagnetization [15]. Fig. 1(b) represents the ac demagnetization method. I on the y-axis is the current passing through the magnetizing coil and T on the x-axis

Manuscript received November 2, 2017; revised January 8, 2018; accepted February 7, 2018. Date of publication February 27, 2018; date of current version September 28, 2018. This work was supported in part by the National Natural Science Foundation of China under Grant 51277122 and Grant 51577122 and in part by the Doctoral Program of the Ministry of Education of China under Grant 20122102130001. This paper was presented in part at the 2016 IEEE 8th International Power Electronics and Motion Control Conference, Hefei, China, May 22–26, 2016. Recommended for publication by Associate Editor Juergen Biela. *(Corresponding author: Baodong Bai.)*

Z. Chen was with Shenyang University of Technology, Shenyang 110870, China. He is now with the School of Electric Engineering and Automation, Hefe University of Technology, Hefei 230009, China (e-mail: chenzw_sygd@126.com).

B. Bai and D. Chen are with the School of Electrical Engineering, Shenyang University of Technology, Shenyang 110870, China (e-mail: baidongbai@163.com; chendezhi_1934@126.com).

W. Chai is with the School of Electrical Engineering, Shenyang University of Technology, Shenyang 110870, China, and also with the Department of Electronic Systems Engineering, Hanyang University, Sangrok-gu 426-791, South Korea (e-mail: chaicool@163.com).

Color versions of one or more of the figures in this paper are available online at http://ieeexplore.ieee.org.

Digital Object Identifier 10.1109/TPEL.2018.2809588

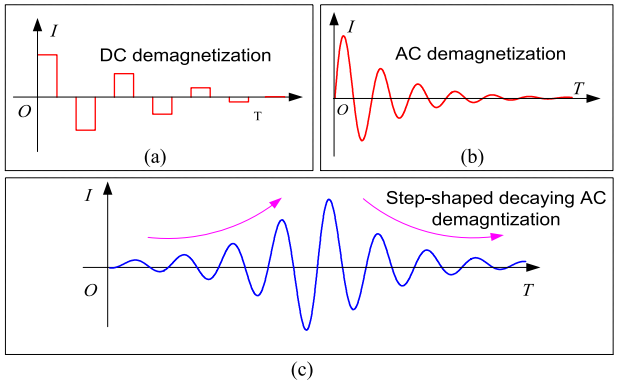

Fig. 1. Demagnetization methods. (a) DC demagnetization. (b) AC demagnetization. (c) Step-shaped decaying ac demagnetization.

denotes the time. But it cannot be ignored that the ac demagnetization has the skin effect and it is difficult to remove the residual magnetism of the internal material.

It is well known that the power transformer is a crucial device for the power transmission. But its running state is often affected by the dc component in the power system. The invasion of dc may cause the rise of neutral point potential in the transformer. As a result, there is magnetic saturation in the core and excitation current distortion in the winding at every half-cycle, which causes some serious hazards in the transformer, such as leakage flux increase, metal structure loss increase, local overheat, insulation damage, noise increase, and vibration intension [16]. Therefore, it is necessary to study the dc bias and how to realize its elimination. There have been some studies about the dc bias restraint in the transformer [17]–[19]. For example, transformer grounding via small resistance [20], electric potential compensation method [21], and blocking capacitance in the neutral line of the transformer to limit the dc bias current [22]. However, the impact of dc bias has not been solved from the aspects of the transformer design.

For the several dc bias treatment methods described above, there exist some limitations, unreliability, and additional pressure on the system. For example, changing the neutral grounding mode of the transformer will lead to the change of the transformer line impedance. The series resistance in the transformer neutral line will generate a large power loss. The blocking capacitance will also change the zero sequence impedance of the transmission system. Meanwhile, it has a low economy and practicality for dc bias treatment. For the reverse injection current scheme, it often requires larger compensation current for the dc bias and multiple grounding poles need to be created in the transformer substation resulting in high building and operating cost [20], [22]. In [23], an electric excitation regulation method is adopted for the inrush current mitigation. This electric excitation regulation method has some guiding significance for dc bias treatment, but the working process of MD requires continuous electricity relying on the auxiliary winding energized by the converter, which increases the complexity and cost of the devices undoubtedly [23]. So far, there is no treatment measure that is effective to eliminate dc bias invasion without changing the transformer external structure and guaranteeing the neutral point of transformer grounding effectively.

In this paper, a novel dc bias treatment method was presented for the transformer combined with the designed hybrid power supply based on a nanocomposite. Under the steady dc magnetizing field, the dc bias can be effectively compensated through the material own remanence. When the dc bias disappears, one step-shaped decaying ac demagnetizing field would be applied to the nanocomposite material. Fig. 1(c) shows the proposed step-shaped decaying ac demagnetization method. The amplitude of the demagnetization field increases first and the magnetic domains of the magnetic material are disrupted, then the amplitude of the demagnetization field decreases slowly. The material would finally return to the magnetic neutral state. Transformer keeps normal working in a small dc or no dc bias environment.

II. Nanocomposite Magnetic Material Property

A. Nanocomposite Magnetic Material

Nanocomposite permanent magnet material combines the characteristics of the higher saturated anisotropy field of the hard magnetic materials and the high saturation magnetization intensity of the soft magnetic materials. They are viewed as two important intrinsic properties to reflect the performance of magnetic materials [24], [25]. But the magnet grains anisotropy field and the saturation magnetization intensity cannot be improved simultaneously. In most cases, the increase of one aspect will inevitably lead to the decrease of the other one. So more and more researchers have begun to composite the soft and hard magnetic phases in order to obtain the composite magnetic material with new performance [26].

Although the magnetocrystalline anisotropy constants of the composite material are very different, the magnetic moment from different orientations at the interface produces the magnetic exchange coupling effect when two magnetic grains are in direct contact. It can prevent the magnetic moment from taking the direction of easy magnetization, and the magnetic moment orientation at the interface continuously changes from one grain easy magnetization direction to another grain easy magnetization direction. Eventually, the disoriented magnetic moment of grain tends to be parallel, which leads to the increase of the magnetic moment along the external magnetic field direction and the remanence enhancement effect [27]. But at the same time, the exchange coupling effect weakens the impact of each magnetic grain's anisotropy so that the effective anisotropy of the grain at the interface decreases resulting in the reduction of the coercivity. It can be seen from Fig. 2, if the material working point is in the first quadrant ($g1$), it is characterized as the soft magnetic property and can be used as the magnetic conductive material. If the material working point is in the second quadrant ($g2$), it is characterized as the hard magnetic property and can be used as the magnetic exciting material.

Based on the nanotechnology and material composite technology, research on the nanocomposite preparation and the magnetic property was carried out in this paper. Blocky nanocomposite magnetic material that meets the technical requirements is prepared. Ultimately, the coercivity range of the magnetic

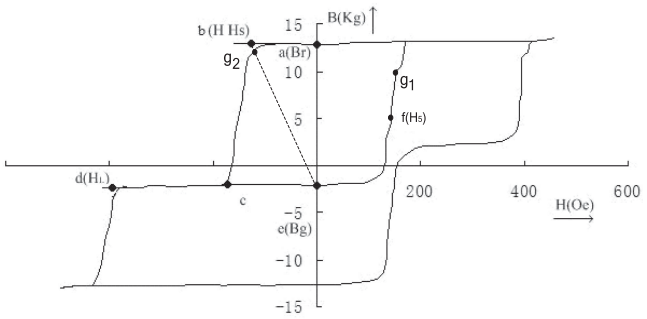

Fig. 2. Hysteresis loop curve of the composite material.

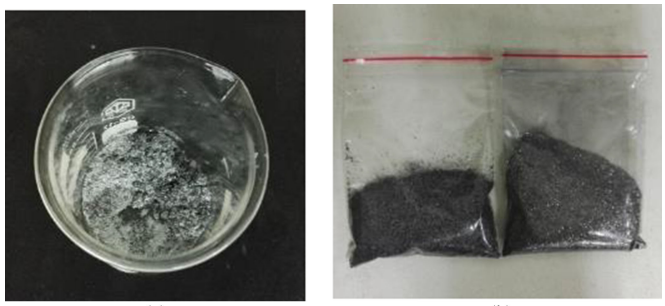

Fig. 3. Adhesive and dried magnetic powder. (a) Adhesive. (b) Magnetic powder.

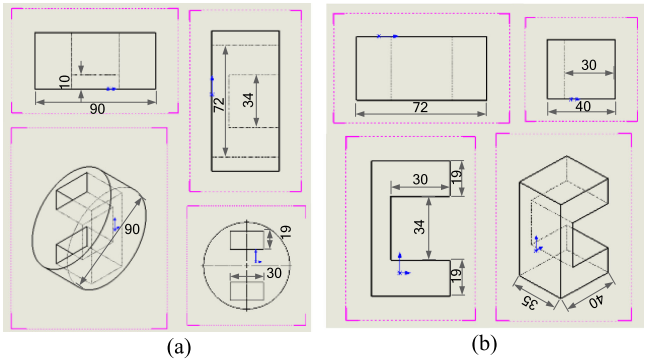

Fig. 4. Mold for the magnetic material and material size. (a) Nanocomposite mold. (b) Shape and size of the material body.

performance is between 930 and 2300 Oe and the remanence range is between 0.3 and 1.2 T. The ability of magnetic conduction and magnetic excitation of the composite material could be converted under the effect of an additional magnetic field.

In terms of the technique, this paper adopted a melt-spinning method to prepare the magnetic powder. Fig. 3(a) shows the adhesive and Fig. 3(b) shows the dried magnetic powder. The magnetic powder prepared is put into the mold and pressed into molding in the hydraulic machine. According to the requirement of the magnet, this paper designs the mold of the material. The specific mold is shown in Fig. 4(a). The shape and size of the material body are shown in Fig. 4(b).

The remanence and coercivity of the nanocomposite are important parameters for the transformer design. The heat

TABLE I
PROPERTY OF THE NANOCOMPOSITE MAGNETIC MATERIAL

Property	Remanence	Coercivity
Property 1	0.34 T	74.57 kA/m
Property 2	0.72 T	131.24 kA/m
Property 3	1.22 T	187.17 kA/m

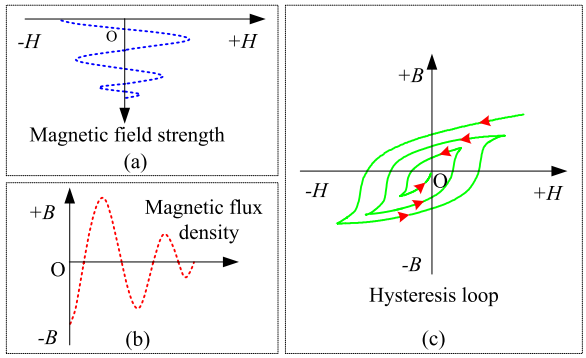

Fig. 5. Schematic diagram of the demagnetization. (a) Magnetic field strength. (b) Magnetic flux density. (c) Demagnetization hysteresis loop.

treatment method was adopted to adjust the property of the nanocomposite. This paper prepares the nanocomposite with three magnetic properties. Table I presents the property of the magnetic material.

B. Magnetic Material MD Method

It is known that when the magnetic material is applied to a dc magnetization coil, the magnetic flux density of the material would increase along the magnetization curve. Because the magnetic materials have a hysteresis effect, the corresponding magnetizing law is relatively complicated. Magnetization of one magnetic material not only depends on the strength of the magnetic field but also has to do with itself original remanence. Before the magnetization, the magnetic characteristic of the material sample is expected to be in the magnetic neutral (O point), as shown in Fig. 5. In this point, the magnetic flux density B is 0 T and there is no residual magnetism. So in this paper, the good magnetization effect of the nanocomposite material is based on a good demagnetization effect [28].

General demagnetization methods select the appropriate ac magnetic field amplitude. The magnetic flux density varies from big to small and the material demagnetization is realized. The method commonly used is to insert the magnet into a magnetizing coil with alternating current. If the external field changes repeatedly between positive and negative value and its amplitude decreases to 0 T gradually at the same time, the magnetized state of the magnet will change along a hysteresis loop, which becomes smaller and smaller, as shown in Fig. 5(c). Finally, when the current drops to zero, the magnetic domain will have no clear magnetization direction. It returns to the magnetic neutral state. Fig. 5 shows the schematic diagram of the demagnetization principle [10].

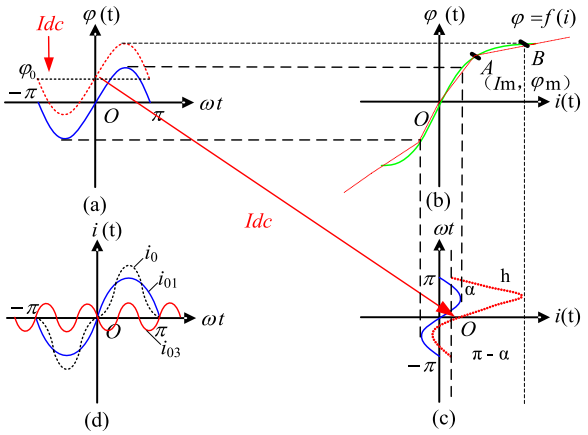

Fig. 6. DC bias formation mechanism.

III. DC Bias Compensation Structure Design

In the design process of the power transformer, the transformer rated working point is usually designed between point O and point A in the magnetization curve shown in Fig. 6(b). After the dc bias, the dc magnetic flux φ_0 and the ac magnetic flux φ superimpose, which makes one half-cycle magnetic flux density increase greatly and the other half-cycle magnetic flux density reduce. The excitation current wave presents as a peak wave and the positive and negative half-cycle waves are not symmetric anymore, changing from Fig. 6(a) to (c). In order to highlight the distortion process of exciting current, the core hysteresis loop is usually ignored and the core nonlinear saturation characteristic is represented by the two pieces of the broken line shown in Fig. 6(b). The slope of the line segment O-A is k_1, which indicates the linear segment of the magnetized curve. The slope of line segment A-B is k_2 indicating the saturation segment of the magnetization curve. In this way, the excitation current waveform obtained from the broken line type magnetization curve could keep the high effectiveness. The current waveform retains the main characteristic of the original excitation current [29], [30].

In Fig. 6, i is the excitation current, i_m is the base frequency excitation current, i_h is the additional excitation current of magnetic saturation, i_b is the dc bias current, I_m is the peak value of current, I is the effective value, φ is the magnetic flux, ω is the angular frequency, and t is the time. The ordinate of two broken lines intersection point is (i_m, φ_m). The magnetic saturation degree h and the included angle α, respectively, indicate the saturation depth of the core and the initial angle of the distorted excitation current.

The total excitation current i_f can be represented as the current sum of three parts including the dc bias current i_b, the normal base frequency excitation current i_m, and the magnetic saturation additional excitation current i_h. The base frequency excitation current $i_m = I_m \sin(\omega t)$. The magnetic saturation additional excitation current i_h in the range of $\alpha \le \omega t \le \pi - \alpha$ can be expressed as

$$i_h = (h-1)\left(I_m \sin(wt) - I_m + I_b\right). \tag{1}$$

In the other range of 0–2α, $i_h = 0$. The dc components contained in the magnetic saturation additional excitation current are

$$I_d = \frac{(h-1)}{2\pi}\left[2\sqrt{I_b\left(2I_m - I_b\right)} - (\pi - 2\alpha)\left(I_m - I_b\right)\right]. \tag{2}$$

Total dc current in the excitation current I

$$I = I_d + I_b. \tag{3}$$

Above-mentioned formula is equal to the dc current component flowing into the transformer winding by the neutral line. It is also possible to deduce the peak of the excitation current, the effective value of excitation current, the base frequency component, and the expression of each current harmonic component shown in Fig. 6(d).

For the dc bias, different types and structure transformers have different abilities to withstand dc bias. The dc bias impact on the transformer is related to its core and winding structure. For example, the sensitivity degree for the dc bias intrusion from large to small is the single-phase (1-1) transformer, three-phase three-column (3-3) transformer, and three-phase five-column (3-5) transformer. The 3-3 transformer is not sensitive to the bias current, since there is no magnetic path for dc bias in the transformer core. DC bias only can be returned from the oil or the fuel tanks and other structural components. But the magnetic resistance of these parts is bigger, so the dc bias magnetic flux is small. However, dc bias in the 3-5 transformer forms current loop through the side choke. The cross section of the magnetic flux return path is small; thus, the core saturation may appear under the low magnetic flux density. The dc bias impact is relatively obvious. For the 1-1 transformer, because each phase would provide a low magnetic resistance path for the dc current, the influence of dc bias is most obvious, which the allowable current is minimal. Therefore, there are strict limits on the dc current allowed to pass. There is the same situation in the three-phase group transformer [29].

Considering the 3-3 transformer is allowed to pass through a larger dc current, detailed study of dc bias compensation for the 1-1 transformer, 3-5 transformer, and three-phase group transformer is carried out in this paper. The schematic diagram of two transformer dc bias magnetic compensation structures is presented in Fig. 7. Fig. 7(a) shows the dc bias magnetic compensation method for the 1-1 transformer. Fig. 7(b) shows the dc bias magnetic compensation method for the 3-5 transformer.

In Fig. 7, the red arrow is the dc bias magnetic flux and the pink arrow is the compensated magnetic flux produced by the nanocomposite. From Fig. 7, it can be seen that the direction of the dc bias flux and the material flux is opposite. The dc bias compensation purpose can be achieved. In order to achieve the above-mentioned compensation structure, a reasonable structure design is essential for the dc bias compensation. Considering the consistency of the analysis ideas of the magnetic circuit and the electric circuit, all-loop Ohm's law can be applied when the magnetic circuit is analyzed

$$\Phi = BS = \mu HS = \mu \frac{NI}{l} S = \frac{NI}{l/(\mu S)} = \frac{F}{R_m} \tag{4}$$

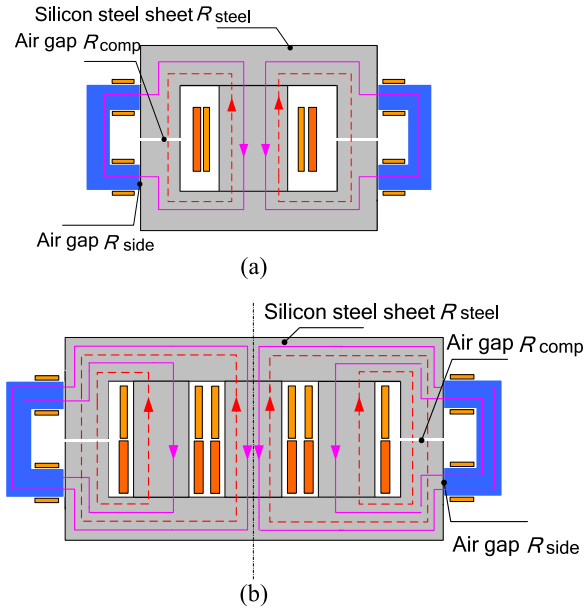

Fig. 7. DC bias compensation structure diagram. (a) 1-1 transformer. (b) 3-5 transformer.

where $R_m = l/(\mu S)$ is the magnetic reluctance, F is the magnetomotive force, l is the average length of the magnetic path, S is the cross section of the magnetic path, and N and I are the turn numbers and the current of the winding, respectively. It is known that the magnetic flux is inversely proportional to the magnetic reluctance. The larger the reluctance, the less the flux passes through. In the transformer core, the compensated flux without flowing into the side leg should flow along the opposite direction of the dc bias flux in the center leg. The most reasonable strategy is to increase the magnetic reluctance of the transformer side leg.

This paper adopts opening an air gap in each side leg, as shown in Fig. 7. It can be seen clearly that the nanocomposite works on two side legs of the transformer. The magnetizing coil is designed on the C-type nanocomposite core, which is used to compensate the dc bias flux. For the three-phase group transformer, it is composed of three identical 1-1 transformers. The main flux of each phase has its own independent magnetic circuit. The dc bias treatment method can refer to the 1-1 transformer dc bias. The specific approach is not covered here. The compensation structure of the 1-1 transformer is designed in detail below.

The flux from the nanocomposite flows through the transformer side leg or the center leg and it depends on the air gap reluctances R_{comp} and R_{side}. And R_{steel} is the reluctances of the silicon steel sheet. The equivalent numerical models of the power transformer under different conditions were analyzed and established, which lay a foundation for the electromagnetism design.

Due to the bilaterally symmetric structure, a half-model is analyzed. Fig. 8 shows the equivalent magnetic circuit of the half-transformer model. F_{ac} and F_{dc} are the ac and dc magnetomotives. F_c is the compensating magnetomotive. The condition of ac and dc excitation is discussed.

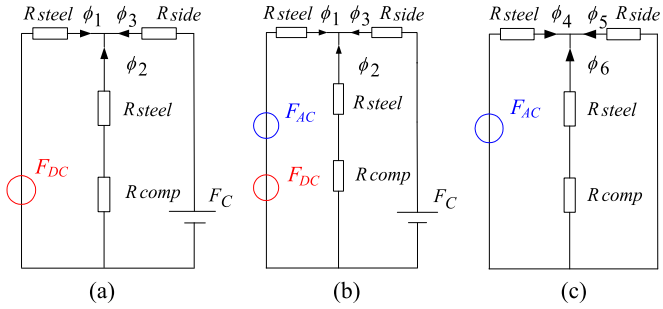

Fig. 8. Equivalent magnetic circuit. (a) DC excitation. (b) Half-model of the magnetic circuit. (c) AC excitation.

TABLE II
RESULTS OF THE AIR GAP IN THE TRANSFORMER

Type	Length of R_{comp}	Length of R_{side}	Length of the material magnetic circuit
220 V/10 kV/10 kVA	0.3–1.0 mm	0.4–0.7 mm	128 mm

Based on the Kirchhoff law, the equivalent magnetic circuit of a half-magnetic circuit model under dc bias excitation is

$$\begin{cases} F_{\text{dc}} = \phi_1 \left[R_{\text{steel}} + (R_{\text{steel}} + R_{\text{comp}}) \,//\, R_{\text{side}}\right] \\ F_C = \phi_2 \left[R_{\text{side}} + (R_{\text{steel}} + R_{\text{comp}}) \,//\, R_{\text{side}}\right] \\ \phi_1 + \phi_2 + \phi_3 = 0 \end{cases} \tag{5}$$

where φ_1, φ_3 are the dc magnetic flux. The equivalent magnetic circuit under ac excitation is

$$\begin{cases} F_{\text{ac}} = \phi_4 \left[R_{\text{steel}} + (R_{\text{steel}} + R_{\text{comp}}) \,//\, R_{\text{side}}\right] \\ \phi_5 R_{\text{side}} = \phi_6 \left(R_{\text{steel}} + R_{\text{comp}}\right) \\ \phi_4 + \phi_5 + \phi_6 = 0 \end{cases} \tag{6}$$

where φ_5, φ_6 are the ac magnetic flux. Let φ_2, $\varphi_4 = 0$, the length of R_{comp} and R_{side} can be calculated. This paper designs two 220 V/10 kV/10 kVA transformers. Table II presents the air gap opening results of the transformers.

IV. MD CIRCUIT DESIGN BASED ON SINGLE-PHASE RECTIFIER AND INVERTER CIRCUIT

A. Relationship Between the Demagnetization Frequency and the Demagnetization Effect

The influence of the demagnetization frequency on the demagnetization effect is mainly reflected by the eddy current loss. The eddy current cannot be carried out like the current in the conductor and it would cause material heat and energy loss. As a result, the energy used to change the material internal magnetic domain decreases. The efficiency of demagnetization would reduce. So it is necessary to select the appropriate demagnetization frequency to reduce the eddy current loss as far as possible. In an alternating magnetic field, because the change of the magnetic flux density B lags behind the change of the external magnetic field, the amplitude of B would wear off from the ferromagnetic surface to the ferromagnetic inside. There is almost no magnetic field in the ferromagnetic conductor. The

magnetic field exists only in a thin layer on the surface of the ferromagnetic conductor. The existence of the skin effect will produce a certain influence on the demagnetization effect [31].

The problem of eddy current and the skin effect can be handled by Maxwell equations. It is assumed that there is an alternating magnetic field along the y-axis in the surface of the ferromagnetic conductor. The magnetic flux density, the magnetic field strength, and the eddy current of the ferromagnetic conductors can be obtained according to the boundary conditions. Basic equations can be simplified as follows:

$$\frac{\partial \vec{H}_y}{\partial x} = J_z, \quad \frac{\partial Jz}{\partial x} = \frac{\mu\mu_0}{\rho}\frac{\partial H_y}{\partial t}. \tag{7}$$

Among them, H is the magnetic field strength. J is the eddy current density. ρ is the resistivity. μ is the vacuum magnetic permeability $4\pi \times 10^{-7}$. μ_0 is the relative permeability of the ferromagnetic medium. Here, H_y and J_z are only related to x. And simplify J_z

$$\frac{\partial^2 H_y}{\partial x^2} = \frac{\mu\mu_0}{\rho}\frac{\partial H_y}{\partial t}. \tag{8}$$

In (8), H_y is a function of x and t. The unique solution, which meets the requirements of the physical, can be obtained as

$$H_y(x,t) = H_0 e^{-bx} e^{j(\omega t - bx)} \tag{9}$$

where $b = \sqrt{\frac{\omega\mu\mu_0}{2\rho}}$ (> 0). This is the magnetic field distribution in the ferromagnetic conductor.

Therefore, the magnetic field intensity H_y spreads along $H = H_0$ on the surface. At the point x on the surface, there is the magnetic field strength

$$H_m(x) = H_0 e^{-bx}. \tag{10}$$

The phase of the magnetic field strength H_y lags behind bx. Define the skin depth as

$$d_s = 1/b = \sqrt{2\rho/(\omega\mu\mu_0)} = 503\sqrt{\rho/(\mu f)}. \tag{11}$$

The physical interpretation of the skin depth is that the amplitude of the magnetic field would decrease as $1/e$ $(e = 2.718)$ of the boundary when it spreads at the depth of $x = d_s$.

Equation (11) shows that the skin depth of the ferromagnetic conductor is directly proportional to the square root of the resistivity and is inversely proportional to the square root of the magnetic permeability and frequency. The distribution of the eddy current in the ferromagnetic conductor is

$$J_z = \frac{\partial H_y}{\partial x} = -b(j+1) H_0 e^{-bx} e^{j(\omega t - bx)}. \tag{12}$$

As for the effect of eddy current loss on demagnetization, the decrease rate of demagnetization efficiency caused by eddy current loss is the error of demagnetization efficiency caused by the eddy current. It is approximately equal to the ratio of the eddy current loss energy to the ac demagnetization magnetic energy in a cycle [31]. The energy density of the ac magnetic field $\omega = B_m^2/2\mu_0$. Therefore, the decrease rate of demagnetization efficiency should be $P_e T/\omega \times 100\%$. For the cylindrical sample magnetic material, the average power loss is

$$P_e = \frac{1}{2}\frac{\pi^2 \mu_0 f}{\rho} r_0^2 \times 100\%. \tag{13}$$

It can be seen that the loss is proportional to the alternating magnetic field frequency f and the material size r_0. So in order to reduce the eddy current loss for the demagnetization effect, it is required to reduce the frequency of the magnetic field.

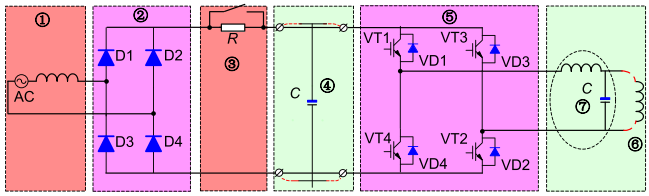

Fig. 9. Schematic diagram of direct-current and alternate-decay-current. (1) Equivalent power supply. (2) Rectifier. (3) Limiting circuit. (4) Capacitor. (5) Inverter. (6) Magnetization coil. (7) Filter circuit.

B. Single-Phase Rectifier and Inverter Circuit

In order to complete the dc bias compensation, this paper designs a direct-current and alternate-decay-current hybrid integrative power supply for magnetic state adjustment of the nanocomposite. Fig. 9 shows the hybrid power supply schematic diagram [32].

Its working principle is described briefly as follows. First, the value of the dc bias current and the direction should be determined when the dc bias occurs. If the direction of the dc bias current is downward, the left rectifier circuit provides compensation current by the combined action of VT1 and VT2. Similarly, if the direction of the dc bias current is upward, it is the combined action of VT3 and VT4. The rectified current creates a reverse compensation flux, which is in the opposite direction of the dc bias flux and equal to the dc bias magnetic flux. After the magnetization operation, the nanocomposite can eliminate the dc bias flux by making full use of the nanocomposite remanent magnetism. When the dc bias disappears, the inverter circuit creates an attenuation alternating current, which increases at first and then decreases until to 0 A by the combined action of VT1–VT4 controlled by the sinusoidal pulse width modulation (SPWM) wave. It can demagnetize the nanocomposite material and restore the power transformer to a normal working condition. Fig. 10 shows three kinds of a circuit working state.

In this paper, magnetizing dc current is obtained by the rectifier circuit. The power electronic devices of the diode are chosen as the switching device in the rectifier circuit. The rectifier circuit adopts the single-phase rectifier circuit, which is most commonly used. The detailed discussion was not carried out here. Demagnetizing ac decaying current is realized by the inverter circuit and the insulated-gate bipolar transistor (IGBT) is selected as the switching device. Fig. 11 shows the equivalent circuit diagram of a single-phase bridge inverter circuit. In the bridge inverter circuit, two switching devices above and below the bridge arm take turns to be ON. Namely, V1 and V2 have the opposite ON–OFF state when they are working. V3 and V4 have the same situation [32], [33]. In the model of the inverter circuit,

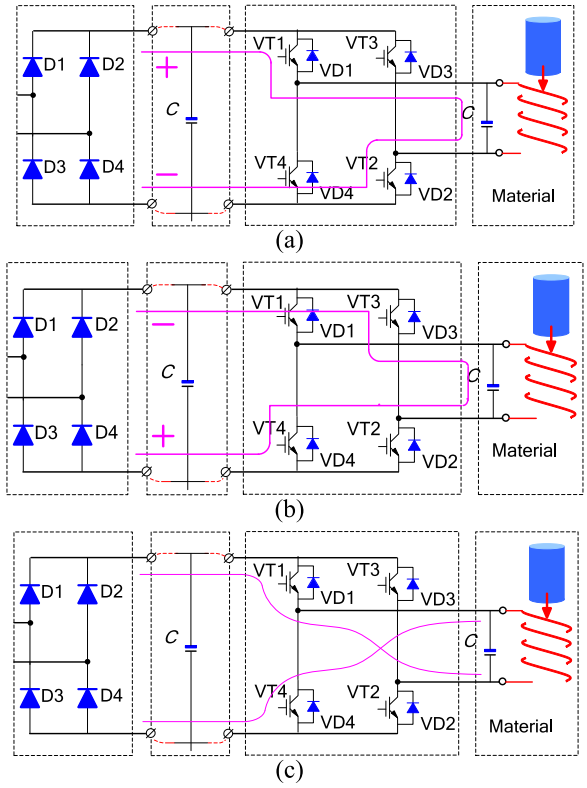

Fig. 10. Three kinds of a circuit working state. (a) Positive magnetizing dc. (b) Reverse magnetizing dc. (c) Alternate-decaying-current demagnetization.

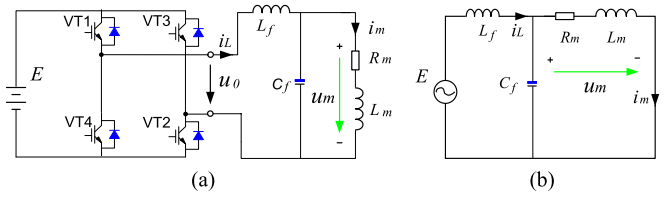

Fig. 11. Single-phase bridge inverter. (a) Main circuit structure diagram. (b) Equivalent circuit of a single-phase inverter.

the power switch devices V1–V4 are seen as an ideal device. L_f and C_f are the output side filter inductance and filter capacitance of the inverter circuit, and R_m and L_m are the equivalent resistance and inductance of the magnetizing coil, respectively. E is the dc bus voltage, and u_0 is the output voltage of the bridge circuit. u_m is the voltage on both ends of the magnetizing coil. i_L and i_m are the current of inductance L_f and magnetizing coil L_m.

The SPWM wave of the demagnetization current formation process is achieved through the following method. The bipolar triangle wave is selected as the carrier wave with the frequency of 2000 Hz. The modulation waves can be achieved by the variation of the frequency and the amplitude. The modulation waves of the two arm bridge control are U_{r1}, U_{r2}, separately. In this paper, the modulation wave adopted the waveform shown in Fig. 12. The detailed formula is

$$U_{r1} = M \times \sin(2\pi f) \tag{14}$$

$$U_{r2} = M \times \sin(2\pi f - 2\pi/3). \tag{15}$$

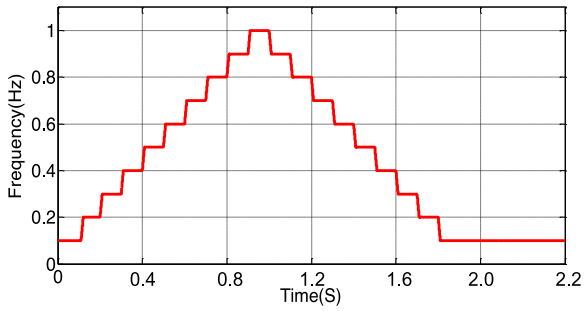

Fig. 12. Amplitude of the modulation wave.

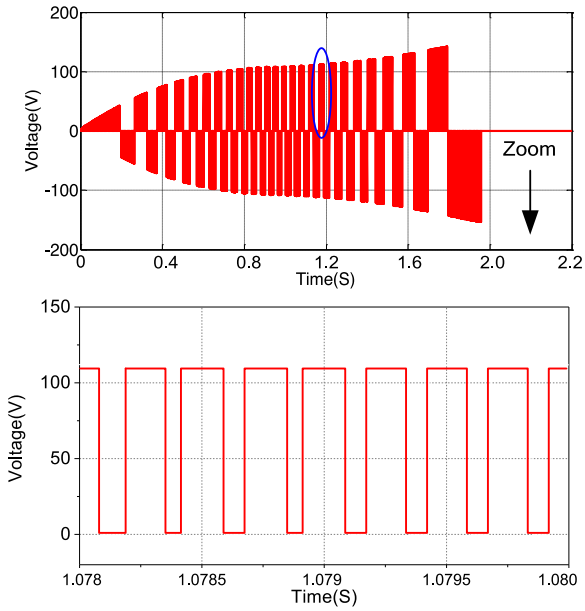

Fig. 13. Voltage of the output on two switch tubes.

The comparative value of the bipolar triangle wave and the modulation waves is switched into the high or low electrical level, which can form the different pulse widths to control the conduction state of four switch tubes. The output voltage of the SPWM inverter can be obtained, as shown in Fig. 13. According to Kirchhoff's law

$$L_f \frac{di_L}{dt} = u_0 - u_m, C_f \frac{du_m}{dt} = i_L - i_m, u_m = L_m \frac{di_m}{dt} + R_m i_m. \tag{16}$$

So the relationship between magnetizing current i_m and magnetizing voltage u_m can be obtained as

$$L_f L_m C_f \frac{d^3 i_m}{dt^3} + L_f R_m C_f \frac{d^2 i_m}{dt^2} + (L_f + L_m) \frac{di_m}{dt} + R_m i_m = u_m. \tag{17}$$

In this paper, the duration time of the alternate-decay-current demagnetization is set to 2 s. In other words, the ac current waveform decays to the end within 2 s and there are 20 attenuation times in 2 s.

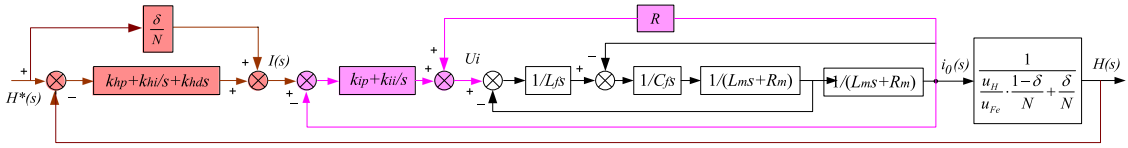

Fig. 14. Structure block diagram of a double-loop control system.

C. Double-Loop Control and Cosimulation Technology

In order to accurately control the magnetic field strength H of the magnetizing coil, which a good MD effect for the magnetic material can be achieved, this paper adopts the double-loop control technology of the magnetic field strength and magnetizing current achieving the nanocomposite magnetic state adjustment. It is assumed that i_m^* is the target magnetizing current, which could produce the above target magnetizing field H shown in Fig. 5. This paper adopts the current proportional-integral regulator to track the current reference signal in order to realize the magnetizing coil current i_m can track i_m^* quickly [34]. As shown in the following equation, in order to eliminate the influence of the voltage of the magnetizing device equivalent resistance R_m on the magnetizing current controller, the expressions of the controller u_m are designed as

$$u_m = k_{ip}\left(i_m^* - i_m\right) + kii\int\left(i_m^* - i_m\right)dt + R_m i_m. \quad (18)$$

Among them, k_{ip} is the proportional coefficient of the current error PI regulator, and k_{ii} is the integral coefficient of the current error PI regulator. Through Laplace transform, the formula can be converted as

$$U_m(s) = \left(k_{ip} + kii/s\right)\left[i_m^*(s) - i_m(s)\right] + R_m i_m(s). \quad (19)$$

According to the expression of the transfer function (19), the equivalent block diagram of the magnetizing current controller can be obtained and is shown as the pink part in Fig. 14

$$\frac{i_m(s)}{i_m^*(s)} = \frac{k_{ip}s+kii}{L_m L_f C_f s^4 + L_m R_m C_f s^3 + \left(L_f + L_m\right) L_f s^2 + k_{ip}s + kii}. \quad (20)$$

As the equivalent inductance L_m of the magnetization coil is a known variable. For the high-order system, the appropriate PI parameters are confirmed based on the pole assignment method, which makes the system have good tracking ability and dynamic performance in the change range of L_m.

A magnetic field strength controller is designed to build the target magnetizing current. The magnetic field strength PID controller with feedforward compensation is designed and is shown as the brown part in Fig. 14, and the target magnetizing current i_m^* can be obtained. H^* is the trajectory of the target magnetic field strength shown in Fig. 5. k_{hp}, k_{hi}, and k_{hd} are the proportional, integral, and differential parameters of the PID controller, respectively. According to (20)

$$\frac{I^*(s)}{H^*(s)} = \frac{\left[u_H/u_{Fe}\cdot(1-\delta)/N+\delta/N\right]\left[k_{hd}s^2+\left(k_{hp}+\delta/N\right)s+k_{hi}\right]}{k_{hd}s^2+\left[k_{hp}+u_H/u_{Fe}\cdot(1-\delta)/N+\delta/N\right]s+k_{hi}}. \quad (21)$$

The appropriate PID regulating parameters of the magnetic field intensity outer loop are confirmed by utilizing the pole assignment method, which ensures the good steady-state precision and good tracking ability of the magnetic field strength in the range of nonlinear variation. According to (20) and (21), the structure block diagram of the double-loop control system can be obtained, as shown in Fig. 14. See (22) shown at the bottom of this page.

The characteristic equation of the control system is $W(s) = Ms^5 + Ns^4 + Rs^3 + Ps^2 + Qs + k_{hi}k_{ii}$. Among them [35]

$$\begin{aligned} M &= \left[u_H/u_{Fe}\cdot(1-\delta)/N+\delta/N\right]L_m L_f C_f \\ N &= \left[u_H/u_{Fe}\cdot(1-\delta)/N+\delta/N\right]L_f R_m C_f \\ R &= \left[u_H/u_{Fe}\cdot(1-\delta)/N+\delta/N\right]\left(L_f+L_m\right)+k_{hd}k_{ip} \\ P &= \left[u_H/u_{Fe}\cdot(1-\delta)/N+\delta/N\right]k_{ip}+k_{hp}k_{ip}+k_{hd}k_{ii} \\ Q &= \left[u_H/u_{Fe}\cdot(1-\delta)/N+\delta/N\right]k_{ii}+k_{hi}k_{ip}+k_{hp}k_{ii}. \end{aligned} \quad (23)$$

The transformer with the dc bias compensation function is an integral body integrated by the control system and the transformer ontology. The conventional simulation methods cannot satisfy the actual working condition of the transformer. This paper adopted a cosimulation method using MATLAB, SIMPLORER, and ANSOFT software. At first, the control system model was established in MATLAB and the control algorithm was applied to the control model by the S function. In addition, the main circuit and the control circuit of the control system were established in SIMPLORER. The main circuit power supply is the hybrid integrative power supplies model. The transformer secondary side was designed as an open circuit. The two-dimensional finite element model of the transformer was built based on ANSOFT software. Simulation of the transformer dc bias compensation is studied. The flux density distribution and magnetic lines distribution of the transformer before and after the dc bias compensation were provided in this paper.

Fig. 15 shows two working schemes of the dc bias compensation. Fig. 16 shows the dc voltage output curves used for

$$\frac{H(s)}{H^*(s)} = \frac{k_{hd}k_{ip}s^3 + \left(k_{hp}k_{ip} + \delta/Nk_{ip} + k_{hd}k_{ii}\right)s + \left(k_{hi}k_{ip} + k_{hp}k_{ii} + \delta/Nk_{ii}\right)s + k_{hi}k_{ii}}{Ms^5 + Ns^4 + Rs^3 + Ps^2 + Qs + k_{hi}k_{ii}} \quad (22)$$

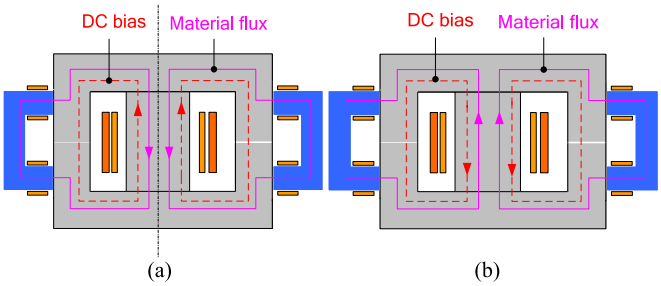

Fig. 15. DC bias generation. (a) State I. (b) State II.

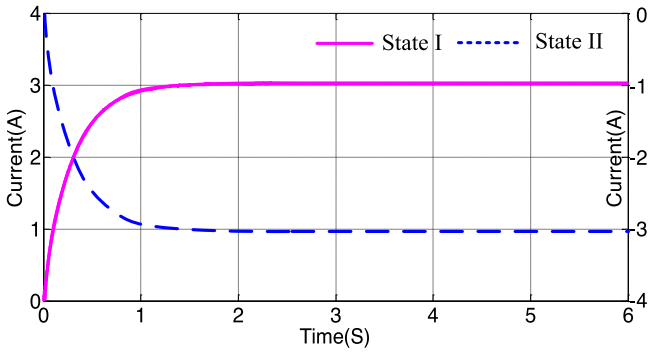

Fig. 16. DC current for the magnetization.

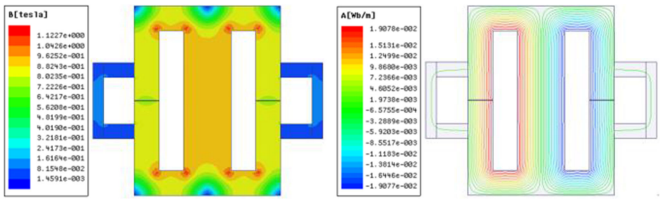

Fig. 17. Transformer flux density distribution and the magnetic lines trend in a normal working state.

producing the magnetizing field. According to the current direction of the dc bias occurrence condition, the compensation is divided into the following two situations.

When the direction of dc bias current is from the bottom to top flowing into the transformer core, the current generated by the power supplies is shown as state I in Fig. 16. The current establishes the magnetizing field to reversely compensate the dc bias flux and reduce or eliminate the dc bias impact. If the opposite event of the dc bias happens, the generated current is shown as state II in Fig. 16. The purpose of reverse compensating dc bias is also achieved.

Based on the cosimulation method, the simulation model was built to verify the correctness and feasibility of the design scheme. The simulation includes three aspects. First, the working magnetic flux was studied when the transformer is running normally. Second, the compensation flux of the magnetic material was analyzed when the material works independently so that it can determine if the direction of the compensation flux is flowing correctly. Finally, after dc compensation, the transformer operation state was observed. When the transformer works normally, the flux density distribution and the trend of the magnetic lines are shown in Fig. 17. It can be seen that the transformer

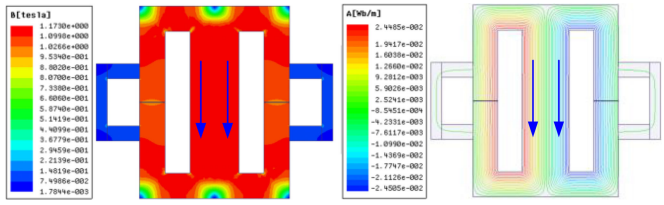

Fig. 18. Transformer flux density distribution and the magnetic field lines trend in the dc bias condition.

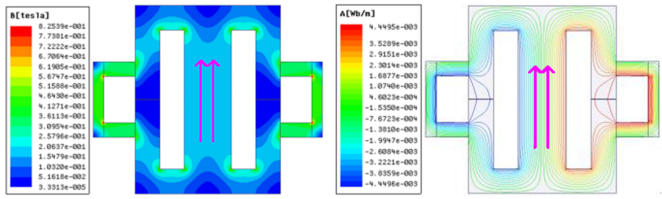

Fig. 19. Flux density distribution and the magnetic field lines trend of the nanocomposite.

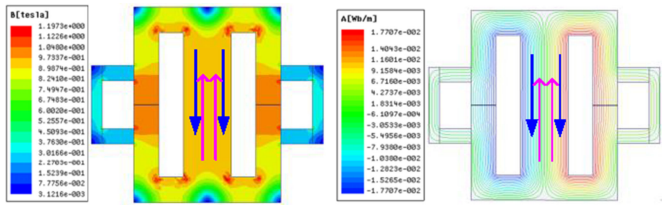

Fig. 20. Flux density distribution and the magnetic field lines trend after dc bias compensation.

ac magnetic flux flowing through the nanocomposite core is almost 0 T. In this way, the demagnetization of nanocomposite core materials caused by the transformer working flux can be effectively avoided.

The flux density distribution and the magnetic lines trend of the transformer dc bias condition are shown in Fig. 18. As it can be seen, the saturation phenomenon of the transformer core occurred and the transformer is divorced from the normal working state.

The flux density distribution and the magnetic lines trend in the transformer core are shown in Fig. 19, when the nanocomposite core works alone. Most of the compensation flux forms a closed loop in the center column and the nanocomposite material, which can effectively restrain the dc bias flux.

After the material compensation, the magnetic flux density distribution and magnetic lines trend results can be seen in Fig. 20. The direction of the compensation flux is opposite to the direction of the dc bias flux. The saturation degree of the transformer core is obviously reduced, and the transformer operation condition obviously improved.

V. Experiment and Result

The hybrid integrative power supply is the essential part for achieving the dc bias compensation. According to the operating condition of the power system, the dc bias current component can be effectively detected. The dc bias in the power system is monitored in real time, which the bias flux can be effectively

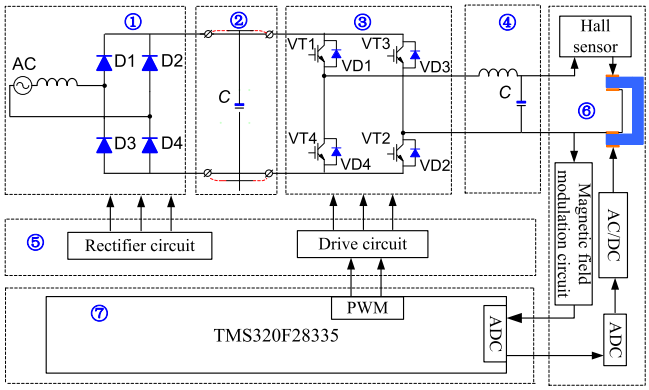

Fig. 21. Hybrid power supply system structure.

compensated. In order to realize the transformer magnetic adjustment, the power supply is built based on a digital signal processor DSP TMS320F28335. The power supply system mainly includes the following seven parts.

1) A rectifier module made up of diodes.
2) Rectifier side filter circuit.
3) Single-phase full bridge inverter circuit composed of the IGBT.
4) Inverter side *LC* filter circuit.
5) Driving circuit of the inverter circuit.
6) Current detection and its signal conditioning circuit.
7) Digital signal processor TMS320F28335, including internal AD sampling and pulse width modulation (PWM) output.

TMS320F28335 is mainly applied to PWM output, analog input, control signal output, and the realization of MD operation. Fig. 21 shows the structure diagram of the hybrid integrative power supply system.

The performance of power conversion circuits is often closely associated with the selected power devices. The unreasonable parameters of the power device may not only reduce the power supply indexes but also affect the reliability of the power supply. Therefore, it is crucial to select the appropriate power device in the design of power electronic products. In this paper, the power switching device of the rectifier circuit of the MD power supply system adopts the rectifier diode because of its simple circuit and low working frequency. The common diode can be satisfied with the rectifier circuit. The single-phase rectifier bridge module of MDQ30A was adopted in this paper. The module adopts a full-pressed structure, with the advantages of small volume and lightweight, which is often used in the input rectifier power supply of the PWM converter. The power switching device of the inverter circuit of the MD power supply system adopts the IGBT, a composite power switching device, which has dual characteristics of bipolar power transistor and MOSFET. It has the advantages of simple control mode, low power loss, and rapid reaction speed, which are applicable to a wide range of frequency and large capacity.

In order to develop the MD ability of the dc and ac hybrid power supply as large as possible, the hard phase of the nanocomposite could show the best magnetic properties state and make the diode; the IGBT power switching device can be satisfied with different levels of magnetic materials MD operation; the highest coercivity 187.17 kA/m is set as the calculation standard in this paper. As long as the biggest coercivity could meet voltage class, the power device can meet requirements of all magnetic materials' property. The relative permeability of the transformer silicon steel sheet is generally located in the range between 7000 and 10 000. The magnitude of the vacuum permeability μ_0 is $4\pi \times 10^{-7}$ H/m. In this paper, the turn number of the MD coil is 1500, and the effective length of closed magnetic path l is 1.14 m. The effective distance between N pole and S pole δ is 0.55 m. From the following formula, we obtain

$$i_0 = \left(\frac{\mu_0 \left(S_{Fe} - S_H \right) + \mu_H S_H}{\mu_{Fe} S_{Fe}} \cdot \frac{1-\delta}{N} + \frac{\delta}{N} \right) \cdot H_\delta \approx 50 \text{ A}. \tag{24}$$

Considering the 3–5 times overload and the safety factor, the rated current value is 156 A. Infineon FF200R17KE3 IGBT is chosen as the power tube. Its rated current is 200 A and the withstand voltage value is 1600 V. The comprehensive performance of this module is very superior, and it is also the main component of the inverter circuit dc/ac. Similarly, the magnetizing current for the other two materials is 20 and 30 A. In the experiment, a suitable magnetic property will be selected for the dc bias compensation [35].

The output waveform of the inverter circuit is just the waveform of PWM modulation, which contains the fundamental harmonic and a large number of high harmonics without the filter circuit. In order to avoid the impact of high harmonics on the MD coil, an appropriate filter must be set on the output side to filter out the high harmonics contained. The output side filter of the inverter is not only to filter out the unnecessary high-frequency components but also to reduce the transmitted power loss as much as possible. The *LC* second-order low-pass filter without loss is generally selected, which presents low impedance characteristic for low frequency and high impedance characteristic for high frequency. It also has no voltage drop of fundamental wave.

According to the design of the hybrid power supply, the sampling frequency of DSP28335 is set as 5 kHz. The cutoff frequency of the filter is 500 Hz. The filter inductance $L_f = 14.5$ mH and the filter capacitance $C_f = 24\,\mu$F. Fig. 22 shows the main hardware components of the power supply system.

The design of the magnetizing coil is the key to achieve the good MD effect. The change of magnetization intensity in the magnetizing coil should be even and slow, so that the magnetic intensity vector can be redistributed. Actually, there is no demagnetization method that could realize the ideal state of the magnetic material with no residual magnetism. Designers are concerned with the method that has the smallest residual magnetism. The magnetic resistance of the ferromagnetic material serving as a closed magnetic circuit in the magnetizing coil is small because the ferromagnetic material has high saturation magnetic flux density B_s, high magnetic permeability μ_m, and smaller intrinsic coercivity H_{cj}. The less energy the space of the magnetizing coil consumed, the stronger the magnetic field

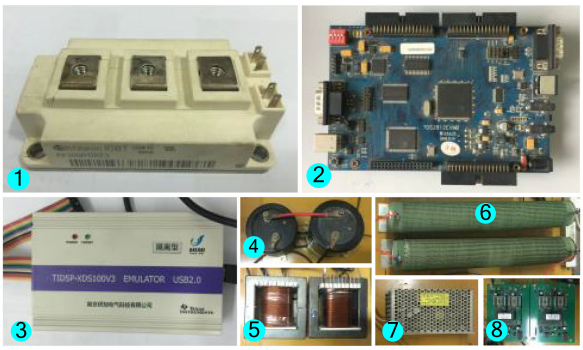

Fig. 22. Hardware components of the power source systems. (1) FF200R17KE3 IGBT. (2) Main control chip TMS320F28335. (3) DSP-XDS100V3 simulator. (4) and (5) Filter capacitance and inductance of output. (6) Partial resistance of the load side. (7) DC power supply. (8) Two-way drive plate.

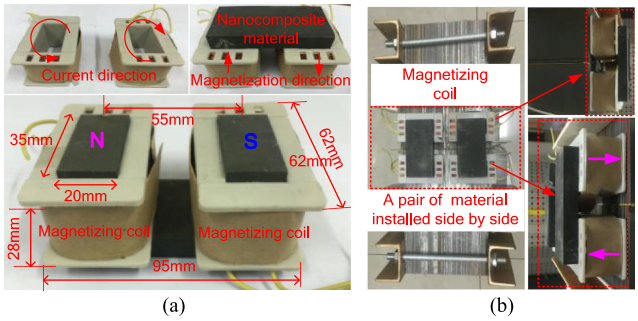

Fig. 23. MD coil and nanocomposite arrangement. (a) MD coil. (b) Specific arrangement of nanocomposite and MD coil.

strength could be used for magnetic material demagnetization. According to the dc bias compensation method, the transformer body is utilized as part of the magnetic circuit loop in which the reluctance of the magnetic circuit can be reduced. The specific dimensions of the MD coil are as follows: the magnetic coil section size is $35 \times 20\,\text{mm}^2$, the extreme distance is 55 mm, and the magnetization winding consists of two sets of enameled magnet wire coil in series, each coil has 1500 turns. Fig. 23(a) shows the MD coil and the nanocomposite arrangement.

Transformer dc bias compensation experiment was designed based on the nanocomposite material. In this paper, a pair of the magnetic materials is installed on left-side and right-side legs of the transformer for dc bias compensation. The amount of dc bias compensation can be improved. Fig. 23(b) shows the specific arrangement of nanocomposite and MD coil.

In order to realize dc bias events and compensation experiment, this paper designs an experimental system to imitate dc bias. The excitation current and harmonics of the power transformer before and after the dc bias were tested and analyzed. Fig. 24 shows the experimental system. In the experiment, an imitating circuit using two transformers with the same parameter is designed, which the primary side is in parallel and the secondary side is in series opposing. The back electromotive force in the secondary side can be counteracted so that the dc source can be introduced into the secondary side, and the dc current is adjusted by adjustable resistance.

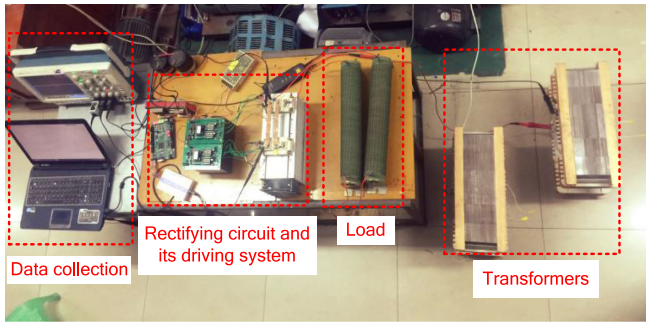

Fig. 24. Experimental system figure.

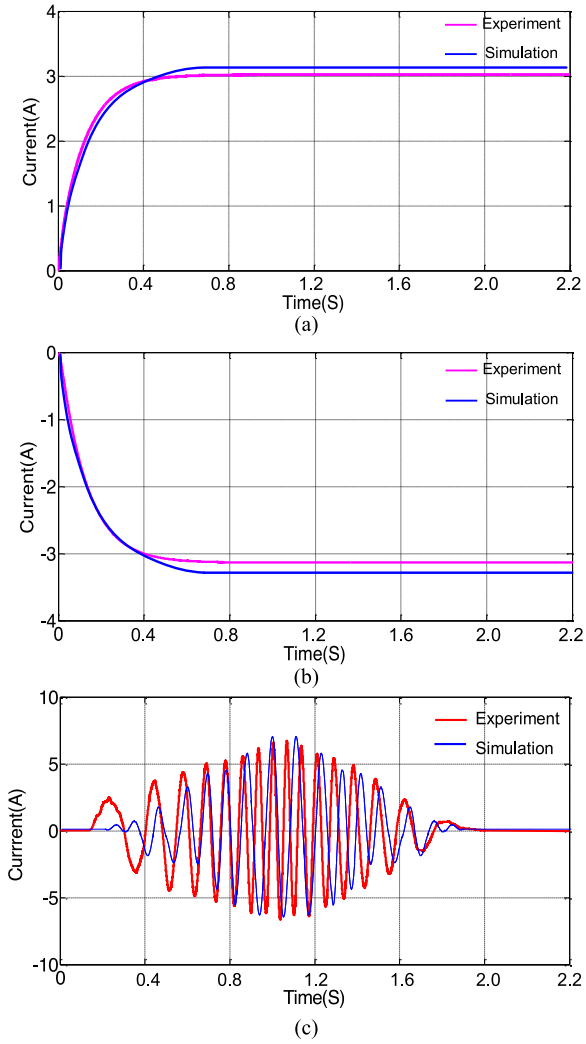

Fig. 25. Steady MD current curve. (a) Positive dc magnetizing current. (b) Reverse dc magnetizing current. (c) Step-shaped decaying ac demagnetizing current.

Fig. 25(a) and (b) shows the comparison of the dc magnetizing current between the simulation and the experiment. Fig. 25(c) shows the ac demagnetizing current curve obtained from the simulation and the experiment. From the comparisons, it can be seen that the results of the experiment and simulation remain fairly consistent. In the power converter, when the ac voltage of 220 V is fed, the maximum required current pulse can reach up

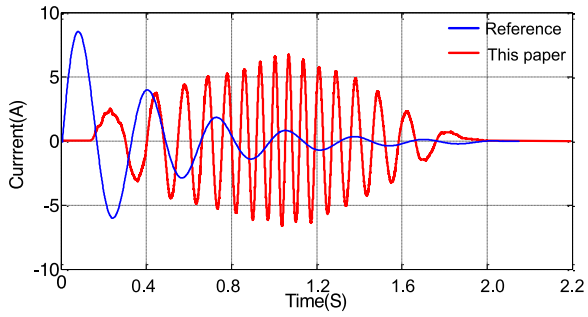

Fig. 26. Two kinds of the ac demagnetization method.

to 50 A, and the power rating of the power converter approximate to 7.8 kW. The steady dc magnetization and decaying ac demagnetization from the hybrid integrative power supplies are good, which lay important guarantee for adjusting the magnetic state of the nanocomposite and lay a good foundation for dc bias compensation.

In this paper, the comparison between the traditional ac demagnetization and the proposed step-shaped decaying ac demagnetization method was carried out. Owing to the fact that anisotropic NdFeB magnet cannot be completely demagnetized relying on ac demagnetization given in [28] shown in Fig. 26, further demagnetization operation may be required. Sometimes, multiple ac demagnetization or thermal demagnetization is needed for the complete demagnetization, which may cause damage and bring pressure to the equipment. At the same time, the current would cause the magnetic material heating during the process of multiple ac demagnetizations, which will affect the usage life.

In order to ensure the uniform variation of the magnetic flux density, the duration of the demagnetization process is also important. For different magnetic materials, the appropriate duration should be selected according to their own properties. For a good demagnetization effect, the change of magnetization intensity is required to be uniform and slow to ensure that the magnetization vector can be redistributed. The maximum amplitude of demagnetization should reach the magnetic field value of saturation magnetization. The lower the frequency of the demagnetization curve and the slower the amplitude varies, the better the demagnetization effect it would have. In this paper, 10 Hz is selected for the demagnetization frequency. The step-shaped decaying ac current varies 20 times in 2 s and then the decaying process comes to the end. It can be seen from Fig. 27(a), the demagnetization precision with high frequency is not easy to control, and the demagnetization effects may vary widely. Choosing the low frequency is suitable for the ac demagnetization. And the low-frequency magnetic field is easier to control and has a quite good repeatability. Fig. 27(b) indicates that ac demagnetization cannot satisfy the requirement of $H = 0, B = 0$. Compared with the demagnetizing curve of the traditional ac demagnetization method shown in Fig. 27(b), the step-shaped decaying ac demagnetization method has a better demagnetizing effect.

Table III shows the comparison of the excitation currents before and after the compensation when dc bias current is 0.3,

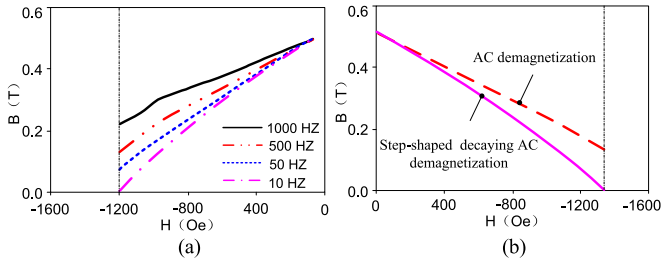

Fig. 27. Demagnetizing curve of the nanocomposite. (a) Demagnetizing curve in a second quadrant at different frequencies 10, 50, 500, and 1000 Hz. (b) Demagnetizing curve of two ac demagnetizing methods. $B(T)$ is the unit of the magnetic flux density, and H(Oe) is the same as H (kA/m), which is the unit of the magnetic field strength. There is such a conversion relationship $1\,\mathrm{kA/m} = 4 * \pi$ Oe. In this paper, Oe is utilized to represent the unit of the material coercivity uniformly.

TABLE III
COMPARISON OF THE POWER TRANSFORMER EXCITATION CURRENT BEFORE AND AFTER COMPENSATION

DC bias current (A)	Normal working	DC bias	Postcompensation size	Compensation amount (%)
$I_{dc} = 0$	4.63	–	–	–
$I_{dc} = 0.3$	4.63	7.80	5.17	33.72
$I_{dc} = 0.6$	4.63	13.65	9.72	28.79
$I_{dc} = 1.0$	4.63	18.74	15.13	19.26

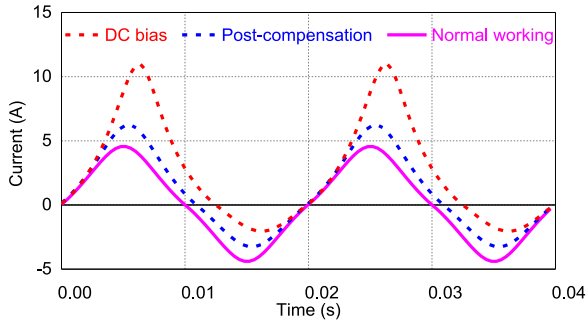

Fig. 28. Exciting current distribution before and after dc bias compensation.

0.6, and 1.0 A. It can be seen that after the application of the magnetic material, the transformer excitation current has a noticeable falling and the purpose of transformer magnetic state adjustment has been achieved. Under the condition of 0.3 A dc bias, 33.72% of the maximum compensation is achieved. But it should be noted that with the increase of dc bias current, dc bias compensation ability decreases, which may be mainly due to the limit of the magnetic energy of the nanocomposite.

Figs. 28 and 29 show the excitation current before and after the compensation when the dc bias current is 0.3 A; it can be seen that the transformer excitation current waveform moves up, the peak value of positive half-wave increases, the peak value of negative half-wave decreases, and the harmonic content increases when the dc bias occurs. Compared to the traditional ac demagnetization method in [36], it can be seen that the harmonics are obviously improved in the low-frequency domain. This is because the proposed step-shaped decaying ac demagnetization method has a good material magnetic state adjustment

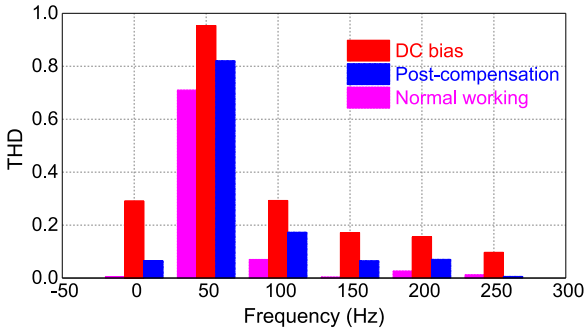

Fig. 29. Harmonic distribution before and after dc bias compensation.

effect. The transformer excitation current and excitation current harmonic content have a significant decline. The feasibility and correctness of the design are further verified through the experimental results.

VI. Conclusion

According to the magnetic exchange coupling effect, this paper put forward a hard and soft magnetic phase nanocomposite material, which is suitable for the electromagnetic equipment. Based on the nanocomposite combined with magnetic resistance theory, novel transformer structure with dc compensation ability was presented. It can realize the inverse compensation of the dc bias magnetic flux by controlling the remanence of the material. The transformer does not change its connection mode and effectively ensures transformer grounding, which has advantages of simple structure, rapid compensation, and low energy cost.

Based on the characteristics of the nanocomposite to the external magnetic field, one kind of direct-current and alternate-decay-current hybrid integrative power supply was proposed. It is used for the material magnetic property adjustment and can realize the effective transformation between hard phase and soft phase, which could lay a good foundation for the subsequent effective regulation of the core magnetic state. Double-loop control and cosimulation technology were adopted in this paper; simulation of the transformer field-circuit in different states was conducted, which verified the correctness and feasibility of the design.

In the last section, MD power supply system was designed and two 220 V/10 kVA power transformers were manufactured. The MD experiment and dc bias compensation experiment were completed. The experimental results show that the simulation results are in good agreement with the experimental results. The direct-current and step-shaped decaying ac current output can achieve a good MD effect for the magnetic material. DC bias occurred in the transformer core can be effectively compensated. The hybrid power supplies designed in this paper can offer some valuable guidance to the research and application of MD. It can be also used in other locations for the magnetic materials MD. Finally, what needs to be pointed out is this paper is an extension of a conference paper presented at the 2016 IEEE 8th International Power Electronics and Motion Control Conference (IPEMC-ECCE Asia). The authors abandon the original rectification method and propose a new single-phase supply power of rectifier and inverter circuit. The amplitude of the demagnetization field increases and then decreases slowly and it can achieve a better demagnetization effect [36].

References

[1] N. Fernando and F. Hanin, "Magnetic materials for electrical machine design and future research directions: A review," in *Proc. IEEE Int. Electr. Mach. Drives Conf.*, May 2017, pp. 1–6.

[2] L. Ferraris, F. Franchini, and E. Pošković, "Hybrid magnetic composite (HMC) materials for sensor applications," in *Proc. IEEE Sens. Appl. Symp.*, Apr. 2016, pp. 1–6.

[3] A. Krings, M. Cossale, A. Tenconi, J. Soulard, A. Cavagnino, and A. Boglietti, "Magnetic materials used in electrical machines: A comparison and selection guide for early machine design," *IEEE Trans. Ind. Appl.*, vol. 23, no. 6, pp. 21–28, Sept. 2017.

[4] Y. Li, Q. Zhao, L. Wang, C. Zhang, and R. Yan, "Improved high-frequency rotating magnetic properties tester for nanocrystalline soft magnetic material," *IEEE Trans. Magn.*, vol. 53, no. 11, Sept. 2017, Art. no. 6101504.

[5] N. Fernando, G. Vakil, P. Arumugam, E. Amankwah, C. Gerada, and S. Bozhko, "Impact of soft magnetic material on design of high-speed permanent-magnet machines," *IEEE Trans. Ind. Electron.*, vol. 64, no. 3, pp. 2415–2423, Mar. 2017.

[6] C. Ó. Mathúna, N. Wang, S. Kulkarni, and S. Roy, "Review of integrated magnetics for power supply on chip (PwrSoC)," *IEEE Trans. Power Electron.*, vol. 27, no. 11, pp. 4799–4816, Jun. 2012.

[7] Y. Sheng, W. Eberle, and Y Liu, "A novel EMI filter design method for switching power supplies," *IEEE Trans. Power Electron.*, vol. 19, no. 6, pp. 1668–1678, Nov. 2004.

[8] A. Lizaro, A. Barrado, J. Pleite, J. Vdzquez, and E. Olfas, "New approach of average modelling and control for ac/dc power supplies which operates with variable duty cycle," in *Proc. Power Electron. Spec. Conf.*, Jun. 2004, pp. 652–658.

[9] Y. Li and J. Zheng, "A low-cost adaptive multi-mode digital control solution maximizing ac/dc power supply efficiency," in *Proc. Appl. Power Electron. Conf. Expo.*, Feb. 2010, pp. 349–354.

[10] K. Berger, B. Gony, B. Douine, and J. Lévêque, "Magnetization and demagnetization studies of an HTS bulk in an iron core," *IEEE Trans. Appl. Supercond.*, vol. 26, no. 4, Jan. 2016, Art. no. 4700207.

[11] J. Zou, M. D. Ainslie, D. Hu, and D. A. Cardwell, "Mitigation of demagnetization of bulk superconductors by time-varying external magnetic fields," *IEEE Trans. Appl. Supercond.*, vol. 26, no. 4, Feb. 2016, Art. no. 8200605.

[12] S. Högberg, F. B. Bendixen, N. Mijatovic, B. B. Jensen, and J. HolbØll, "Influence of demagnetization-temperature on magnetic performance of recycled Nd-Fe-B magnets," in *Proc. IEEE Int. Electr. Mach. Drives Conf.*, May 2015, pp. 1242–1246.

[13] M. Soinski, "The method of summation used for calculating demagnetization state in flat magnetic materials," in *Proc. IEE Colloq. Meas., Model. Imag. Non-Destruct. Test.*, London, U.K., Mar. 1991, pp. 7/1–7/6.

[14] T. M. Baynes, G. J. Russell, and A. Bailey, "Comparison of stepwise demagnetization techniques," *IEEE Trans. Magn.*, vol. 38, no.4, pp. 1753–1758, Jul. 2002.

[15] A. E. Goldshtein, S. A. Kalganov, and E. I. Urazbekov, "Demagnetization method for dimensional steel units," in *Proc. 8th Russian-Korean Int. Symp. Sci. Technol.*, Jul. 2004, pp. 217–219.

[16] B. Tekgun, Y. Sozer, and I. Tsukerman, "Measurement of core losses in electrical steel in the saturation region under dc bias conditions," *IEEE Trans. Ind. Electron.*, vol. 53, no. 1, pp. 88–89, Aug. 2017.

[17] Y. Yao, C. S. Koh, G. Ni, and D. Xie, "3-D nonlinear transient eddy current calculation of online power transformer under dc bias," *IEEE Trans. Magn.*, vol. 41, no. 5, pp. 1840–1843, May 2005.

[18] O. Bíró1 *et al.*, "Finite element analysis of three-phase three-limb power transformers under dc bias," *IEEE Trans. Magn.*, vol. 50, no. 2, Feb. 2014, Art. no. 7013904.

[19] B. Zhang, X. Cui, R. Zeng, and J. L. He, "Calculation of dc current distribution in ac power system near HVdc system by using moment method coupled to circuit equations," *IEEE Trans. Magn.*, vol. 42, no. 4, pp. 703–706. Apr. 2006.

[20] J. Zhao, "Restrain transformer dc bias via grounding small resistance," *Autom. Electr. Power Syst.*, vol. 30, no. 12, pp. 88–91, Jun. 2006.

[21] Z. Pan *et al.*, "Potential compensation method for restraining the dc bias of transformers during HVdc monopolar operation," *IEEE Trans. Power Deliv.*, vol. 31, no. 1, pp. 103–111, Feb. 2016.

[22] Z. Du, "Test and analysis on restraining transformer dc bias by changing electric potential of grounding grid," *High Voltage Eng.*, vol. 32, no. 8, pp. 69–72, Aug. 2006.
[23] J. Burkard and J. Biela, "Transformer inrush current mitigation concept for hybrid transformers," in *Proc. 19th Eur. Conf. Power Electron. Appl.*, Sept. 2017, pp. P.1–P.9.
[24] A. Manaf, M. Al-Khafazi, P. Z. Zhang, H. A. Zavies, R. A. Buckley, and W. M. Rainforth, "Microstructure analysis of nanocrystalline Fe-Nd-B ribbons with enhanced hard magnetic properties," *J. Magn. Magn. Mater.*, vol. 128, no. 3, pp. 307–312, Dec. 1993.
[25] B. G. Kelly and K. M. Unruh, "Preparation and magnetic properties of submicrometer sized Sm-Co powders prepared from nanostructured precursor oxides," *IEEE Trans. Magn.*, vol. 49, no. 7, pp. 3349–3352, Jul. 2013.
[26] K. Fukunaga, J. Kuma, and Y. Kanai, "Effect of strength of intergrain exchange interaction on magnetic properties of nanocomposite magnets," *IEEE Trans. Magn.*, vol. 35, no. 5, pp. 3235–3240, Aug. 2002.
[27] A. Manaf, M. Al-Khafaji, P. Z. Zhang, and H. A. Davies, "Microstructure analysis of nanocrystalline Fe-Nd-B ribbons with enhanced hard magnetic properties," *J. Magn. Magn. Mater.*, vol. 128, no. 3, pp. 307–312, Dec. 1993.
[28] Z. Chen, B. Bai, and D. Chen, "Design and implementation of a novel controllable reactor based on nanocomposite magnetic material," *IEEE Trans. Ind. Appl.*, vol. 51, no. 6, pp. 4464–4469, Nov./Dec. 2015.
[29] X. Li, X. Wen, P. N. Markham, and Y. Liu, "Analysis of nonlinear characteristics for a three-phase, five-limb transformer under dc bias," *IEEE Trans. Power Deliv.*, vol. 25, no. 4, pp. 2504–2510, Oct. 2010.
[30] O. Biro, S. Ausserhofer, G. Buchgraber, K. Preis, and W. Seitlinger, "Prediction of magnetising current waveform in a single-phase power transformer under dc bias," *IET Sci., Meas. Technol.*, vol. 1, no. 1, pp. 2–5, Jan. 2007.
[31] E. I. Urazbekov and A. I. Kornienko, "The method of high performance demagnetization of long-length cylindrical articles," in *Proc. 8th Int. Sci. Pract. Conf. Students, Post-Graduates Young Scientists*, Jul. 2003, pp. 60–62.
[32] F. Wu and J. Zhao, "Current similarity analysis based open-circuit fault diagnosis for two-level three-phase PWM rectifier," *IEEE Trans. Power Electron.*, vol. 32, no. 5, pp. 3935–3945, May 2017.
[33] D. S. Wijeratne and G. Moschopoulos, "A ZVS-PWM full-bridge converter with reduced conduction losses," *IEEE Trans. Power Deliv.*, vol. 29, no. 7, pp. 3501–3513, Jul. 2014.
[34] Y. Liao, "A novel reduced switching loss bidirectional ac/dc converter PWM strategy with feedforward control for grid-tied microgrid systems," *IEEE Trans. Power Deliv.*, vol. 29, no. 3, pp. 1500–1513, Mar. 2014.
[35] P. Xu, *Research on Inverter Based on Apparatus of Magnetization and Demagnetization for Hard Magnetic Material*. Hangzhou, China: China Jiliang Univ., 2013.
[36] Z. Chen, B. Bai, and D. Chen, "Magnetization and demagnetization circuit design applied to transformer dc bias elimination based on three-phase rectification circuit," in *Proc. IEEE 8th Int. Power Electron. Motion Control Conf.*, May 2016, pp. 2223–2228.

Zhiwei Chen (M'14) was born in Anhui, China, in 1988. He received the B.S. degree in measurement and control technology and instrumentation from Liaoning Institute of Science and Technology, Benxi, China, in 2012. He is working toward the Ph.D. degree majoring in electrical engineering at Shenyang University of Technology, Shenyang, China.

His research interests include numerical analysis of electromagnetic field and electromagnetic compatibility in power systems and electronic systems.

Baodong Bai (M'85) was born in Liaoning, China, in April 12, 1955. He received B.S. degree in electrical engineering from Shenyang Institute of Electrical and Mechanical (whose name was changed to Shenyang University of Technology, in 1985), Shenyang, China, in 1982, the M.S. degree in electrical engineering from the Harbin Electrical Institute (which merged with the University of Science and Technology, in 1995), Harbin, China, in 1984, and the Ph.D. degree from Shenyang University of Technology, in 2006.

He is currently a Professor with the School of Electrical Engineering, Shenyang University of Technology. His research interests include engineering electromagnetic field electromagnetic compatibility and permanent magnetic medical actuator.

Dezhi Chen (M'12) was born in Jilin, China, in 1983. He received the M.S. and Ph.D. degrees in electrical engineering from Shenyang University of Technology, Shenyang, China, in 2010 and 2014, respectively.

From 2014 to 2015, he was a Post-Doctor with the Electronic Systems Engineering, Hanyang University, Sangrok-gu, South Korea. In 2016, he was a Visiting Researcher with Hanyang University. He is currently an Assistant Professor with Shenyang University of Technology. His research interests include design and analysis of power transformers and special electric machines.

Wenping Chai was born in Liaoning, China, in 1991. She received the B.S. degree in electrical engineering and automation from the Harbin Institute of Technology, Harbin, China, in 2014. She has been working toward the Ph.D. degree majoring in electrical engineering at Shenyang University of Technology, Shenyang, China, since 2014.

She is currently carrying out research in the Department of Electronic Systems Engineering, Hanyang University, Sangrok-gu, South Korea. Her research interests include design, analysis, and optimization of electric machines.